Journal of Hydrology 625 (2023) 129954

Contents lists available at ScienceDirect

Journal of Hydrology

journal homepage: www.elsevier.com/locate/jhydrol

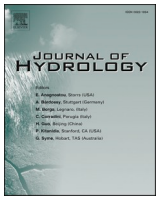

Research papers

Aerial characterization of surface depressions in urban watersheds

Lapone Techapinyawat [a], Ian Goulden-Brady [a], Hannah Garcia [b], Hua Zhang [a,*]

[a] College of Engineering, Texas A&M University-Corpus Christi, Corpus Christi, TX 78412, USA
[b] College of Science, Texas A&M University-Corpus Christi, Corpus Christi, TX 78412, USA

ARTICLE INFO

This manuscript was handled by Huaming Guo, Editor-in-Chief, with the assistance of Lili Yao, Associate Editor

Keywords:
Surface depression
Microtopography
Urban hydrology
Digital elevation model (DEM)
Unmanned aircraft system (UAS)

ABSTRACT

Digital elevation models (DEM) are one of the most fundamental inputs for hydrological modeling. It has been a common practice to remove all surface depressions in a DEM as they are assumed to be data errors. The emerging technology of unmanned aircraft systems (UAS) provides an opportunity to re-examine this assumption at the hyperspatial resolution. This study was the first attempt to characterize small surface depressions in urban environments using UAS imagery. Using an urban area in south Texas as the study site, UAS flights were conducted to yield hybrid DEMs at the resolution of 8–14 cm, coupled with comprehensive ground truth collection. Surface depressions identified from the UAS DEMs were first corrected based on the vertical accuracy of DEMs and then validated through field surveys, with comparisons to two existing LiDAR DEMs (1-m and 10-m). The hydrological impacts of different DEM-derived estimates of catchment depression storage were examined using the Curve Number method across different design storms. Results show that the UAS DEMs outperformed the LiDAR DEMs in describing the microtopographic control of urban overland flow and associated hydrological connectivity across built and natural features. The 8-cm UAS DEM revealed 926% more depression storage than the 10-m LiDAR DEM. This demonstrates a compelling correlation between increasing DEM resolution and enhanced quantification of depression volume. Consequently, the increased depression storage reduced surface runoff by 41% under a two-year design storm and 13% under a 200-year design storm. The results suggest a strong relationship between the DEM resolution and the derived depression estimates, aligning with the fractal nature of watershed systems. Also, the results indicate that the centimeter-level UAS DEMs were not immune from problems. They could yield fake depressions caused by factors such as vegetation, temporary street objects, and underground sewer pipes. The findings of this study suggest the need to quantify the relationships between DEM resolution and associated hydrological attributes and develop new digital drainage analysis algorithms that could effectively incorporate UAS data into urban hydrological modeling.

1. Introduction

The topography of a watershed has a major impact on its hydrological processes (Moore et al., 1991) and controls the movement of surface water and dissolved substances (Paton and Haacke, 2021; Wang et al., 2018). Surface depressions are one of the most common topographic features that have important effects on watershed hydrology (Hu et al., 2020). A surface depression (hereafter, depression) is a region that is lower in elevation than its surrounding areas (Jenson and Domingue, 1988). This characteristic allows depressions to collect and store surface runoff, affecting runoff pathways, the time of concentration, and ultimately the amount of streamflow reaching the outlet (Abd Elbasit et al., 2020; Callaghan and Wickert, 2019; Darboux et al., 2002; Hu et al., 2020; Wang et al., 2021). Depressions have been recognized as a source of complexity in the analysis of rainfall-runoff relationships (Wang and Chu, 2020; Wang et al., 2021) and an important parameter of hydrological models (Dell et al., 2021; Zakizadeh et al., 2022), with important implications for stormwater management and flood mitigation.

Small depressions are not presented in digital elevation models (DEMs) derived from conventional sources because their horizontal resolutions are insufficient. For instance, the horizontal resolutions of United States Geological Survey (USGS) national DEMs, such as the 1990 USGS DEM, which has a resolution of 30 m, and the 2019 3D Elevation Program (3DEP), which has a resolution of 10 m. Such coarse DEM resolutions could eliminate important topographical features (Habtezion et al., 2016), including small depressions that are smaller than a DEM cell (Lindsay and Creed, 2006). These neglected depressions can consist of various natural components (e.g., ponds) and human-

* Corresponding author at: 6300 Ocean Drive, Unit 5797, Texas A&M University-Corpus Christi, Corpus Christi, TX 78412, USA.
E-mail address: hua.zhang@tamucc.edu (H. Zhang).

https://doi.org/10.1016/j.jhydrol.2023.129954
Received 21 December 2022; Received in revised form 5 June 2023; Accepted 13 July 2023
Available online 19 July 2023

made structures (e.g., roadside swales), all essential features of micro-topography in an urban area. This is particularly true for studies in urbanized watersheds using coarse-resolution DEMs.

DEM-derived depressions are assumed to be artifacts that result from input data errors and interpolation techniques (Cordonnier et al., 2019; Jenson and Domingue, 1988) and thus topographical features (Callaghan and Wickert, 2019; Lindsay and Creed, 2005). It has been a common practice to remove all DEM-derived depressions in watershed hydrological analysis (Wang and Liu, 2006). However, this practice is implemented without assessing if some of the removed depressions are real depressions. The chance of mistakenly removing real depressions could be high when using a high-resolution DEM. Depressionless DEMs could depict faulty landscapes, resulting in unrealistic flow estimation (Habtezion et al., 2016) and misconceptions of surface hydrological patterns.

This is particularly important in the emerging use of high-resolution imagery from unmanned aircraft systems (UAS). Throughout the recent decade, various UAS has been increasingly employed to obtain remote sensing data (Nex et al., 2022). Compared to satellites, UAS are operated at considerably lower altitudes and can lead to DEMs with unprecedented spatial resolutions (Singh et al., 2022). Hydrological research has substantially benefited from the breakthrough of UAS technology and the derived DEM products (Abdelkarim et al., 2019; Abedini et al., 2006; Acharya et al., 2021; Deng et al., 2020; Escobar Villanueva et al., 2019; Leitao et al., 2016; McDonald, 2019; Schumann et al., 2019; Trepekli et al., 2022; Velez-Nicolas et al., 2021). In those studies, the spatial resolutions of UAS-generated DEMs vary from millimeters to meters, indicating that the UAS-generated DEMs could be better than spaceborne-generated DEMs in support of urban rainfall-runoff modeling and stormwater management studies. However, confirming the validity of DEMs in accurately representing real depressions is essential for obtaining reliable insights. This is especially pertinent for depressions associated with the intricacies and variations of the surrounding terrain. Thus, correctly identifying and distinguishing between real and fake depressions is necessary for producing precise and dependable data.

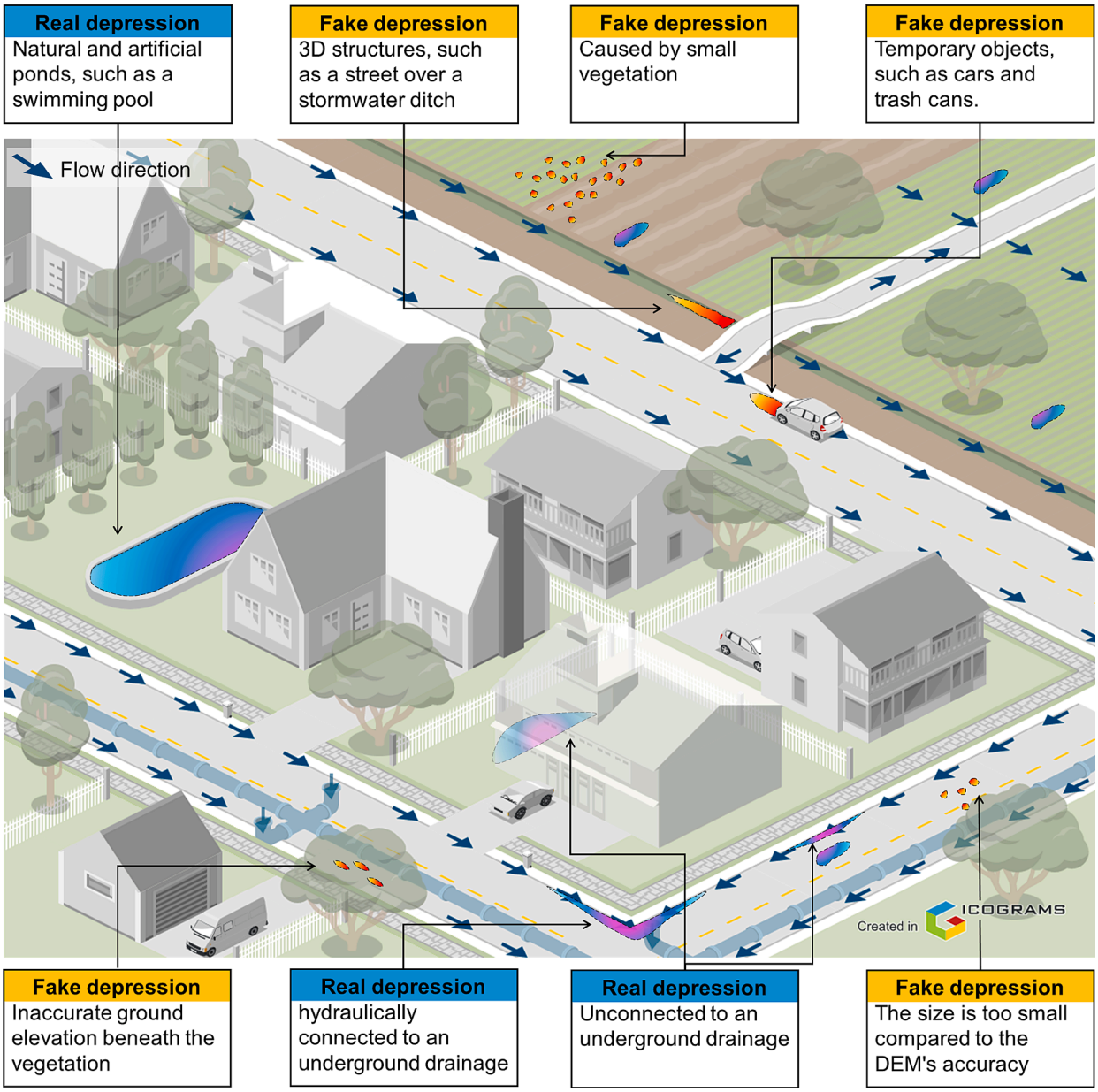

Fig. 1. A conceptual diagram of depressions in urban microtopography. Blue arrows indicate the direction of surface runoff. (For interpretation of the references to color in this figure legend, the reader is referred to the web version of this article.)

Using a typical urban area in south Texas as the study area, the objectives of this study are to: (i) to evaluate whether UAS-derived DEMs could provide an improved description of urban depressions than existing DEMs; and (ii) to explore the relationships between the DEM resolution and the derived hydrological attributes. In doing so, this study examines whether UAS-generated DEMs can accurately characterize and quantify small depressions in urban microtopography. The findings of this study could improve the applications of UAS for urban hydrology, provide insights into the uncertainties of different elevation datasets, and indicate the need for new methods for digital drainage analysis in the era of high-resolution geospatial big data.

2. Materials and methods

The analysis of urban microtopography based on DEMs inevitably involves the identification of real depressions and the exclusion of fake depressions (Fig. 1). Real depressions can include both built structures (e.g., street gutters and swimming pools) and natural features (e.g., small ponds). Fake depression can be caused by factors such as the techniques of DEM generation (e.g., the interpolation algorithm) or the disturbance of artificial objects (e.g., a car parked on the street). Regardless of the DEM resolution, there is always a mixture of real and fake depressions in DEMs of urban environments, which requires demands careful attention in DEM-based urban hydrological studies.

2.1. Study area

The study area is located on the western side of Corpus Christi, Texas, USA, covering an urban area of approximately 0.16 km^2 (Fig. 2a and 2b). Based on the zoning data of the City of Corpus Christi, this area has been developed as a low-density residential district (City of Corpus Christi GIS Services, 2018). It includes a total of 110 single-family houses with an average lot size of 830 m^2. The southern part of the study area is less developed yet, dominated by vacant lots and a mixture of woods and grasslands.

The topography follows a north–south gradient with elevation ranging between 3 m and 22 m above sea level and an average slope of 4.25%. Consequently, surface runoff generally flows northward into the Nueces River, discharging into the Corpus Christi Bay, an estuary of the Gulf of Mexico. The study area is served by a municipal separate stormwater system, but only the northern region has underground stormwater sewers. The stormwater system is entirely gravity driven, and the outlet is located near the northwestern corner of the study area (Fig. 2c).

2.2. Methods

2.2.1. Overview

The study (Fig. 3) was organized into four stages. The first stage, "Data acquisition and processing," involved downloading open-source airborne LiDAR DEMs and generating DEMs from UAS-photogrammetry acquisition. The processed DEMs were analyzed in the second stage, "Digital drainage analysis," using ArcGIS Pro tools to calculate hydrological properties such as depressions, catchment size, and depression storage arising from using different DEMs. These variations could significantly affect the input dataset for hydrological

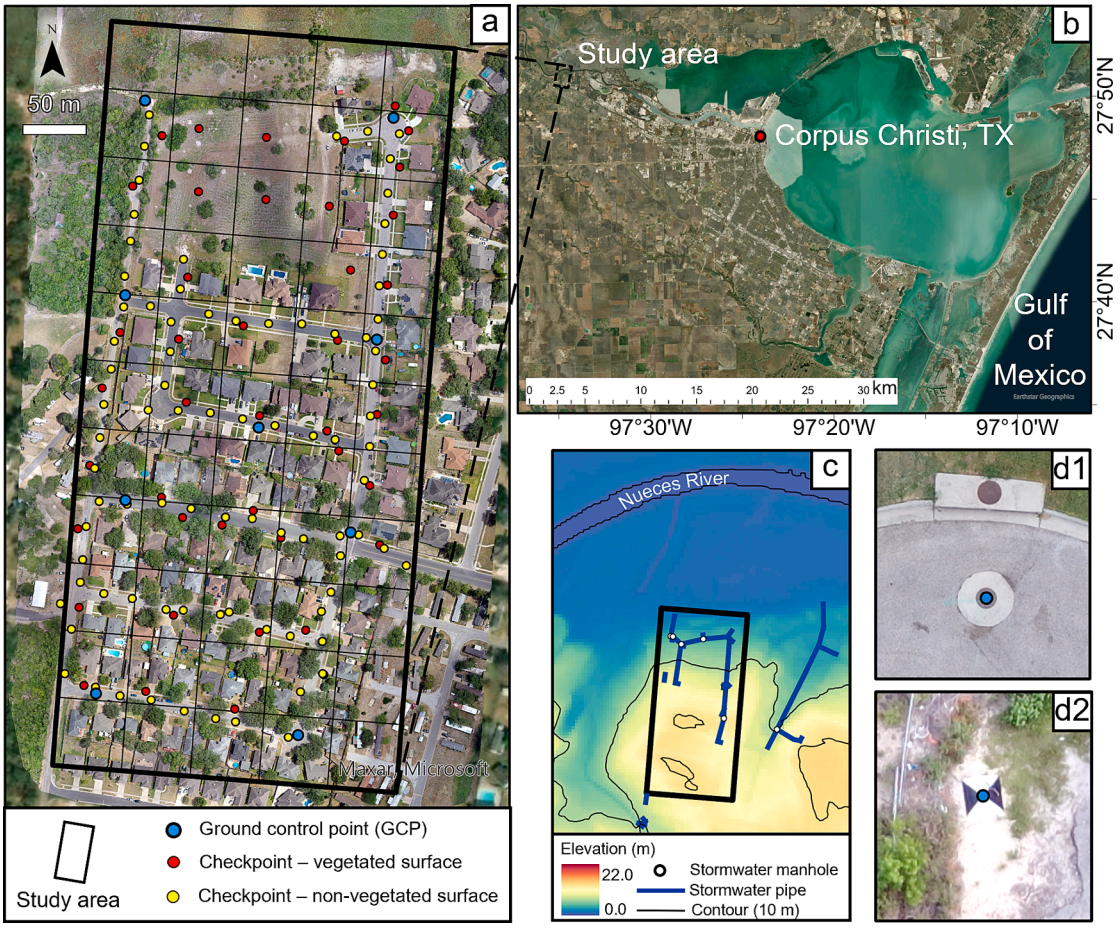

Fig. 2. Study area: (a) data collection; (b) location of the study area; (c) elevation and drainage (blue lines indicating stormwater sewers); (d1, d2) examples of permanent and temporary features for GCP locations. (For interpretation of the references to color in this figure legend, the reader is referred to the web version of this article.)

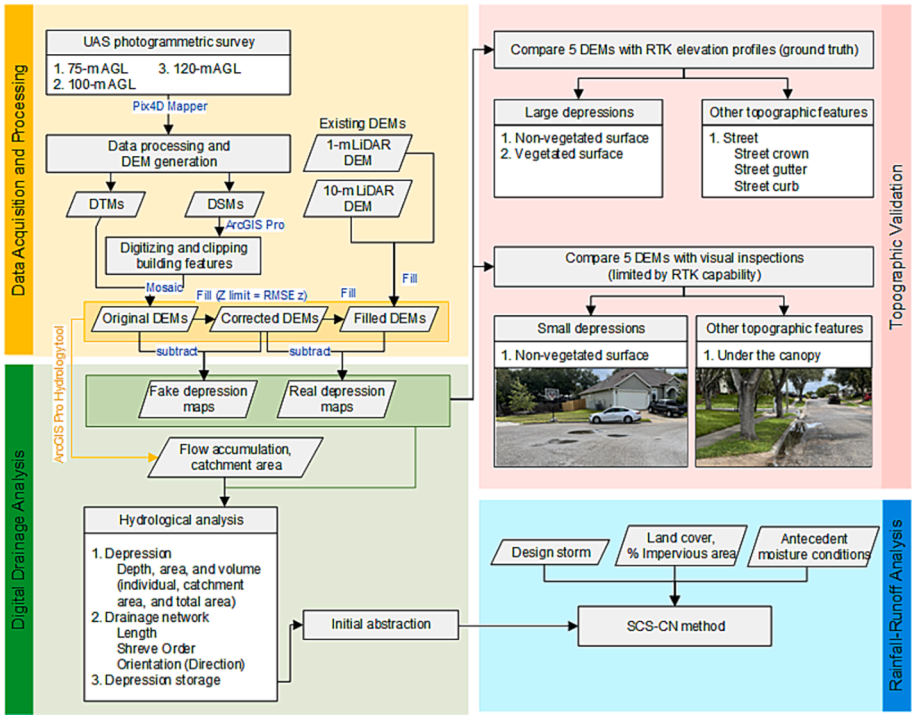

Fig. 3. Research framework. DTM (digital terrain model); DSM (digital surface model).

modeling, ultimately influencing the model's accuracy and reliability. The third stage, "Topographic validation," involved field observations using a real-time kinematic positioning (RTK) system and visual inspection to verify the identified real and fake depressions. This stage ensured that the hydrological properties derived from the DEMs closely represented real-world conditions, enabling more accurate comparisons in the subsequent runoff estimation analysis. In the fourth stage, "Rainfall-runoff analysis," the SCS-CN Method was applied along with initial abstraction and impervious surface estimation for each catchment to assess the runoff estimates derived from the various DEMs for different rainfall scenarios. The comparison aimed to determine the impact of DEM on hydrological modeling and to identify the suitable DEM for the study.

2.2.2. *Data acquisition and processing*

A small UAS (DJI Mavic 2 Pro) was used for aerial imaging. It was equipped with a 20-million-pixel RGB camera and was operated at 75, 100, and 120 m above ground level (AGL), resulting in ground sampling distance (GSD) of 1.60, 2.22, and 2.72 cm, respectively. The frontal and side overlapping values were set at 80% in all three surveys. The weather conditions during all operations were sunny, with 15% cloud coverage. Pix4D Capture was employed for the design and implementation of these aerial surveys.

High-accuracy georeferencing was assured based on ground control points (GCPs) (Padro et al., 2019). A total of nine GCP were systematically established across the study area (Fig. 2a). One GCP was placed in the middle of the study area, and the other eight were placed along the boundary with approximately equal spacing. This uniform distribution of GCPs provides a small error in the DEM (Tonkin and Midgley, 2016). All GCPs were measured using a handheld centimeter-level real-time kinematic positioning system (Trimble TDC 150).

Also, checkpoints (CPs) were established to evaluate how the estimated elevation differs from the true elevation measured by TDC150. A total of 127 CPs were surveyed, covering both pervious and impervious surfaces. A stratified scheme was used to minimize spatial data collection biases. For CPs on pervious surfaces (e.g., vegetation or bare soils), the study area was divided into approximately 54-m square grids, and one CP was established in the publicly accessible land (red dots in Fig. 2a). For impervious surfaces, CPs on were established along the streets or sidewalks at 25-m equal intervals (yellow dots in Fig. 2a).

The UAS images were processed using the Structure from Motion (SfM) technique in Pix4D Mapper. Point cloud densification was set to the scale of the original image size with high point density. The DTM quality was enhanced using a point cloud classification algorithm with geometric and color features (Becker et al., 2018). The inverse distance weighting (IDW) method was used to interpolate the points to obtain the best DEM accuracy (Aguera-Vega et al., 2020). The processing resulted in a digital terrain model (DTM) and a digital surface model (DSM), all standard outputs from SfM analysis.

However, neither the DTM nor DSM was sufficient for urban hydrological analysis. To address this, a hybrid non-vegetated surface DEM (NVS DEM) was created by clipping building surfaces from the DSM and mosaicking them onto the DTM. This NVS DEM represented a compound natural-built surface, which allowed for more realistic modeling of runoff generation and routing across bare earth and building surfaces, as the representation of buildings can create depressions that affect the overland flow network (Leitao et al., 2009). Additionally, the USGS 3DEP (hereafter, 10-m LiDAR DEM) and STX LiDAR DEM (hereafter, 1-m LiDAR DEM), with 10-m and 1-m resolutions, were included for comparison purposes.

The UAS-generated DEMs provide unprecedented high spatial resolutions. However, regardless of their resolutions, the DEMs can still contain fake depressions (Lindsay and Creed, 2006) that should be removed. In this study, the DEMs were corrected by removing suspicious small depressions where the maximum depth was smaller than the DEM's vertical accuracy, i.e., assuming they were too shallow to be true. This assumption on fake depressions concurred with the suggestions from existing studies (Wu et al., 2019; Zandbergen, 2010; Zhao et al., 2022). The vertical accuracy of the DEM in this study was calculated as the root-mean-square error (RMSE) (Cuartero et al., 2005; Gao, 1997; Jiménez-Jiménez et al., 2021) based on the measurements of CPs. Then the calculated RMSE was used as a threshold for filtering fake depressions. This correction process was implemented using the Fill tool in ArcGIS Pro by assigning the value of RMSE to the Z-limit parameter - the

minimum height difference between the lowest point in a depression and its pour point. If the height were less than the RMSE, the depression would be filled and flattened to its pour point. The resulting DEM was noted as "corrected DEM" hereafter.

2.2.3. Digital drainage analysis

ArcGIS Pro Hydrology tools were deployed for digital drainage analysis based on the corrected DEMs. They included: (i) the Flow Direction tool that determines pixelwise flow directions based on the D8 flow algorithm (Jenson and Domingue, 1988); (ii) the Basin Tool that delineates the catchment areas. In this study, this hydrologic attribute refers to the runoff-contributing area; (iii) the Fill tool that removes all depressions in the elevation model by filling algorithm; and (iv) the Flow Accumulation tool that calculates cumulative flow on each cell and locates the area of flow concentration. This attribute is used to access a network delineation to determine where runoff accumulates the most in a particular location. The threshold was set at 0.5 percent of the maximum flow accumulation using the same stream extraction procedure (Zhang and Pan, 2014). The Fill tool was applied twice in this study. The first application was to create corrected DEMs by removing all small depressions that were shallower than the vertical accuracy. The second application was to create filled DEMs (i.e., depressionless DEMs).

The depressions were identified by calculating the elevation difference between the two DEMs, i.e., subtracting the corrected DEMs from the filled DEMs. In this raster of elevation difference, only the pixels of depressions had positive values, representing the elevation change that would be required to remove the depressions. This raster was further used to calculate depressions' geometry, area, and volume. The isoperimetric quotient equation calculated the geometry. This number indicates the circularity of the depressions. The area was calculated as the product between the number of depression pixels and the pixel size. The volume was calculated as the summation of the elevation change of each pixel multiplied by the pixel size.

At this stage, a quantitative analysis of the depressions was performed better to understand the similarities and dissimilarities between the DEMs, providing their respective strengths and limitations in representing depression characteristics. The analysis focused on the distribution (PDF) of depression area, volume, and isoperimetric quotient, which helped evaluate the ability of each DEM to describe the variety of depression sizes, volumes, and shapes. This comparative assessment of the DEMs allowed for a comprehensive understanding of their performance in capturing depression characteristics, which is crucial for accurate hydrological modeling and runoff estimation.

After this detailed quantitative analysis, the total volume of depressions was combined for each DEM in the study area to compare the total modified area and the modified volume referred to as depression storage. This comparison provided insights into the differences in depression storage capacity between the DEMs, further informing the selection of the most appropriate DEM for specific study objectives and requirements. Finally, the depression storage was calculated for each catchment area, ensuring accurate runoff estimates that account for the influence of depressions on runoff generation.

2.2.4. Topographic validation

The RMSE derived from CPs reflected the DEM's vertical accuracy at the scale of individual pixels, but it could fully distinguish real and fake depressions at the level of features. Therefore, comprehensive validation efforts were conducted to verify a number of selected topographical features through two approaches.

The first approach was rigid field measurements along selected transects using the handheld RTK system. The measurements validated selected depressions on non-vegetated and vegetated surfaces and urban topographical features such as street crowns, gutters, curbs, and sidewalks. The field survey approach aimed to measure the actual topography using the RTK system and compare it to the UAS-derived topography at the centimeter scale. This would demonstrate the reliability of the UAS-generated DEM in accurately revealing urban topographical features. This was essential for confirming the real-world existence of the DEM-derived depressions and the derived hydrological parameters, such as flow direction, flow accumulation, and catchment area.

The second approach was visual inspection after a representative rainfall event. This rainfall event had a duration of six hours and a total rainfall depth of 19.6 mm. The study site was visited immediately after this rainfall event, and the locations of ponding water along the streets were recorded to indicate the existence of true depressions. The visual observation was deemed useful because identifying depressions from a DEM relied on elevation and could not incorporate other unidentifiable factors in a DEM. Although not all true depressions could be visually observable timely because of infiltration and evaporation, it is reasonable to accept that the visible depressions are true depressions.

The five DEM-generated depressions were evaluated as part of the validation process, and the results directly impacted each catchment's depression storage estimation and subsequent runoff estimation. We were able to accurately identify the true depressions and ensure accurate hydrological analysis in the following stage by combining field measurements and visual observations. Additionally, contrasting each DEM's capabilities and limitations revealed insights into their abilities to observe and capture various topographical features. This comparison enabled us to decide the suitable DEM for precisely estimating depression storage, which ultimately improved our comprehension of the hydrological processes taking place in the study area.

2.2.5. Rainfall-runoff analysis

To assess the impact of DEM-derived depression storage on runoff estimation in urban areas, we applied the standard Soil Conservation Service curve number (SCS-CN) method with DEM-derived depression storage as the initial abstraction (I_a):

$$Q = \frac{(P + I_a)^2}{P - I_a + S}$$

$$S = \frac{25400}{CN} - 254$$

where Q represents the runoff depth, P is the precipitation depth, S is the potential maximum retention based on the curve number (CN), and I_a is the initial abstraction. All units are in millimeters.

We set I_a equal to the depression storage determined in Section 2.2.3. Therefore, the five DEMs in this study led to five different estimates of I_a for each catchment, allowing for a comprehensive evaluation of the hydrological implications of all DEMs in a consistent modeling framework. Two widely-used values of I_a (i.e., 5% and 20% of the maximum retention capacity S) were also included for comparison. The determination of the composite CN of each catchment used the impervious surface percentage derived from the UAS imagery and the standard CN tables (USDA-SCS, 1986). For all catchments, we used the hydrological soil group C and the average antecedent soil moisture condition (AMC II).

Rainfall data were a set of design storms rainfall intensity–duration–frequency database for the Corpus Christi area, extracted from the National Oceanic and Atmospheric Administration (NOAA) Atlas 14. The 15-min rainfall duration was set based on the estimated time of concentration with consideration of catchment size, slope, and the longest flow path. Rainfall depth was determined for a set of return periods ranging from 2 to 200 years.

We summed the calculated runoff volumes for each catchment to obtain the total runoff volume in the study area. Then, we divided these volumes by the total area to determine each scenario's runoff depth (mm). This facilitated a comparison of runoff estimates from various DEMs, emphasizing the influence of depression storage and DEM quality on runoff calculations.

Urban environments often contain many small depressions resulting

from human influences and natural processes, and these depressions can play a significant role in the initial abstraction and subsequent runoff generation. As the core component of many urban hydrological models, the SCS-CN method has proved to be an effective tool for addressing this unique aspect of urban landscapes in hydrology. The CN method is the core component for surface runoff in many widely used hydrological models such as the Soil and Water Assessment Tool (SWAT) and the Storm Water Management Model (SWMM). More importantly, it is essential to verify the initial abstraction ratio locally and determine the specific conditions under which the commonly recommended value of 0.05 is appropriate (Krajewski et al., 2020). Here we used DEM-derived depression storage as the initial abstraction to examine deeper into depressions' role in urban runoff generation. This approach highlights the importance of verifying the initial abstraction ratio locally and assessing its impact on runoff estimates. We assumed that interception storage might contribute less to the overall initial abstraction in such areas than depression storage. This approach emphasized the role of depression storage in controlling the initial abstraction and runoff generation, allowing us to precisely assess the sensitivity of runoff estimates to depression storage values obtained from different DEMs. Here, we have catchment-specific values of I_a, in contrast to a uniform fraction of S for all catchments. Our method assumes a negligible role of interception storage in the initial abstraction, which is deemed reasonable given the vegetation conditions in our study area.

3. Results

3.1. Digital elevation models

The three UAS surveys at the altitudes of 120 m, 100 m, and 75 m resulted in three DSMs at resolutions of 2.72 cm, 2.22 cm, and 1.60 cm, respectively (Table 1). The resolution of the derived DTM was set to be five times the resolution of the DSM due to the smoothing algorithm of Pix4D Mapper. Therefore, the resolutions of the DTMs were 13.6 cm, 11.1 cm, and 8.0 cm.

Table 1 also shows the accuracies of the five DEMs (i.e., three UAS-derived DEMs and two existing LiDAR DEMs) based on the comparisons of DEM pixel values to field measurements at 127 checkpoints (Fig. 2a). These checkpoints have average horizontal and vertical accuracies of 2 and 3 cm, respectively. The UAS-generated DEMs had vertical RMSEs in the range of 6–7 cm, much lower than that of the coarse-resolution DEMs. However, the resolution of the UAS DEMs did not appear to impact the RMSE. Whereas RMSEs of the 10-m LiDAR DEM had vertical RMSEs of 21.8 cm on a non-vegetated surface and 31.6 cm on a vegetated surface, much higher than those DEMs. Regarding surface types, the non-vegetated surfaces tended to have lower RMSE than the vegetated surfaces for all DEMs except for the 8-cm UAS DEM. The UAS DEMs performed better than the coarser resolution DEMs in describing built structures in an urban environment, particularly in identifying typical urban drainage structures such as street gutters, sidewalks, and stormwater ditches (Fig. 4).

3.2. Results of digital drainage analysis

The process of removing fake depressions altered the elevation values of DEM pixels. The elevation changes in terms of area and volume were fairly consistent among the three UAS DEMs (as shown in red bars in Fig. 5a and 5b). However, the results varied when it came to filling real depressions (indicated by blue bars in Fig. 5a and 5b). The total area of elevation changes in the 1-m LiDAR DEM, approximately 6,000 m^2, was similar to that of the UAS DEMs. Conversely, the filling algorithms did not significantly affect the area and volume of the 10-m LiDAR DEM. In general, as the resolution increased, so did the filled volume. The 1-m LiDAR DEM differed from the UAS DEMs; for instance, the filled volume of the 8-cm UAS DEM was four times larger than that of the 1-m LiDAR DEM. Furthermore, the filled volumes among the three UAS DEMs were not identical. Invoking the fractal nature characterized by scale invariance (Abedini et al., 2006), our research provides new evidence to quantify the relationship between the DEM resolution and the estimated depression volume.

The probability distribution function (PDF) and rug plot analysis (Fig. 5c, 5d, and 5e) of individual depressions revealed various depression characteristics, emphasizing the importance of understanding the variety of depression sizes, volumes, and geometries. The UAS DEMs and 1-m LiDAR had similar area and shape distributions. The similarity of shape distributions among UAS DEMs and 1-m LiDAR DEM indicated that the 1-meter resolution DEM can capture a variety of urban depressions, as centimeter resolution DEMs do. Additionally, the isoperimetric quotient plot indicated that UAS DEMs and 1-m LiDAR DEM observed most shapes have a quotient of 0.78, representing square-shaped depression areas typically captured in one-pixel size depressions. However, 1-m LiDAR differed in volume, as it tended to capture fewer depressions larger than 1 m^3. In contrast, the 10-m DEM cannot capture any small depressions.

In the rug plot, the 1-m LiDAR DEM appeared to capture fewer varieties in depression sizes, which was limited by its cell size. As a result, the finer resolution DEMs, such as the UAS DEMs, could represent a greater variety of depression sizes. For elongated depressions with a smaller isoperimetric quotient, such as depression along street gutters, the 1-m LiDAR DEM performed similarly to the UAS DEMs.

The number of depressions increased when the spatial resolution of DEM was finer, as shown in Table 2. Three DEMs generated from UAS provided different depression and catchment numbers. However, 1-m LiDAR DEM performance in capturing these hydrological attributes was similar to the UAS DEMs. In contrast, the 10-m LiDAR DEM produced significantly fewer depressions and catchment areas, disregarding microtomographic features related to small depressions. Therefore, the 1-m LiDAR DEM performed better than the 10-m LiDAR DEM, enabling it to produce more comparable data.

All five DEMs were derived from the same study area, and despite their differing spatial resolutions, they collectively captured the primary hydrological features and represented similar drainage network structures. However, the 10-m LiDAR DEM, due to its coarser resolution, may overlook some microtopographic features essential to depict drainage networks, particularly in urban environments such as engineered drainage systems. In contrast, the finer resolution DEMs, especially those derived from UAS, captured more intricate details of the microtopography and associated catchment attributes. Consequently, these DEMs provided a more accurate representation of the drainage network, particularly in areas with complex topography.

Table 1
Specifications of different elevation and surface models in this study.

Data	Flight altitude AGL (m)	Point cloud density	Resolution (cm)			Vertical RMSE (cm)	
			GSD, DSM	DTM	NVS DEM	Non-vegetated surface	Vegetated surface
8-cm UAS DEM	75	7581.19/ m^3	1.60	8.0	8.0	6.4	5.5
11-cm UAS DEM	100	1804.17/ m^3	2.22	11.1	11.1	6.9	7.1
14-cm UAS DEM	120	1394.74/ m^3	2.72	13.6	13.6	5.6	7.1
1-m LiDAR DEM	1,700–2,294	2.5/ m^2	–	100	–	8.0	11.9
10-m LiDAR DEM	unknown	unknown	–	1000	–	21.8	31.6

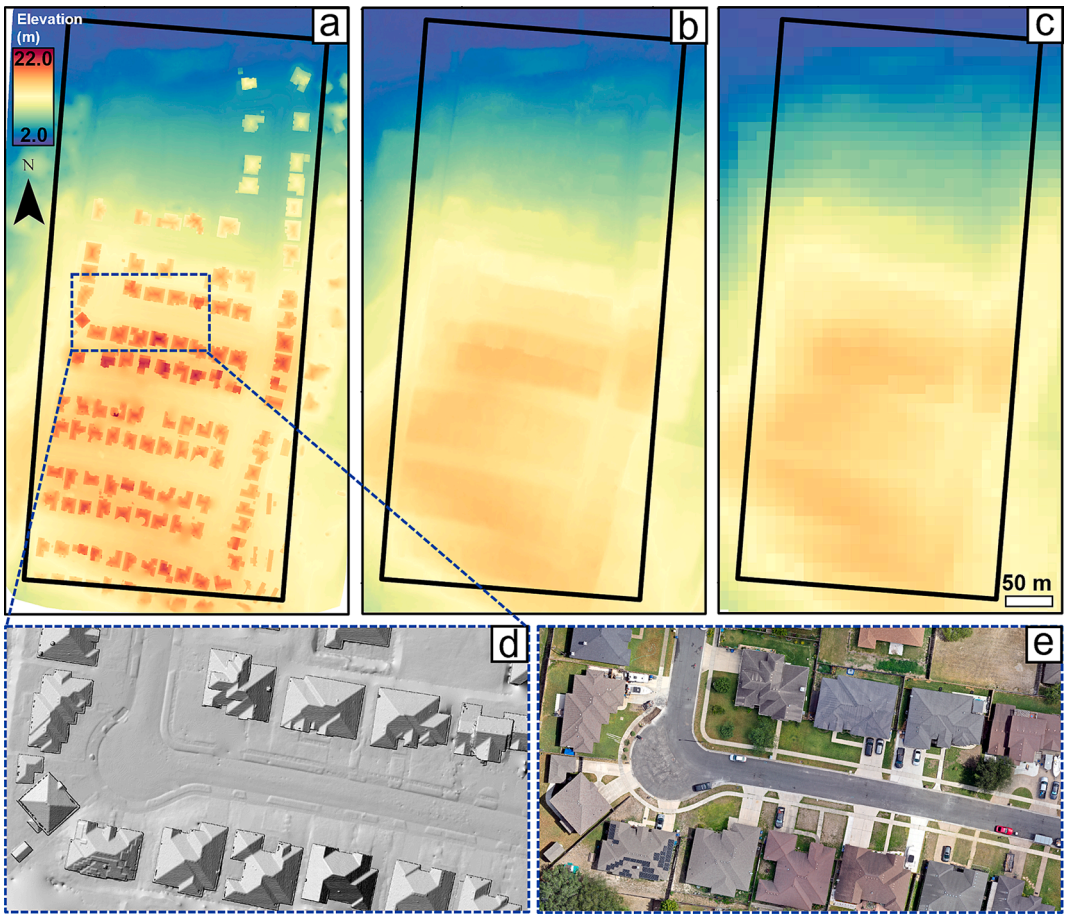

Fig. 4. Comparison of a UAS DEM to existing DEMs. (a) 8-cm UAS DEM; (b) 1-m LiDAR DEM; (c) 10-m LiDAR DEM; (d) the hillshade map from 8-cm UAS DEM; and (e) the orthomosaic map from 8-cm UAS DEM.

While all five DEMs presented similar drainage networks at a broader scale, the finer resolution DEMs (UAS DEMs and 1-m LiDAR DEM) offered improved detail and accuracy in representing hydrological attributes. The UAS DEMs and 1-m LiDAR DEM exhibited similarities in the orientation and location of flow accumulation, with high concentrations appearing along the gutters on both sides of the streets. In contrast, the runoff from the 10-m LiDAR DEM did not exhibit flow along the streets and street gutters, which are the primary drainage system in the study area. Fig. 6 shows that, in comparison to the 10-m LiDAR DEM, the flow accumulation patterns in the UAS DEMs and 1-m LiDAR DEM were typically more precise and consistent with the real world. The 10-m LiDAR DEM exhibits less detailed flow accumulation patterns due to its coarser resolution. This discrepancy in accuracy and detail showed the advantages of adopting finer resolution DEMs for hydrological modeling and analysis, such as UAS DEMs and the 1-m LiDAR DEM.

The depression storage of each catchment was lower in the 1-m LiDAR DEM and 10-m LiDAR DEM due to the exclusion of human-made structures that could collect runoff, such as swimming pools, and horizontal and vertical detail in capturing depression extent and depth. Fig. 7 demonstrates the inconsistent results of all five DEMs in depression storage. Despite being acquired by the same UAS device at slightly different altitudes, the 8-cm UAS DEM still provided a larger depression storage capacity than the coarser-resolution DEMs. Moreover, Fig. 7 demonstrates how the distribution of depression storage capacity varied amongst the DEMs. The depression storage capacity for the 1-m LiDAR DEM appeared to be distributed more evenly, with most catchments lying within the 0 to 5 mm range. In contrast, the finer-resolution DEMs exhibited a more diverse distribution of depression storage capacity across catchments. This variability in depression storage distribution could have implications for estimating catchment runoff. The diverse storage capacities may lead to different runoff predictions depending on the resolution of the DEM used.

3.3. Results of validation

Here we show the results of three validations based on RTK measurements. The first validation focused on a street segment and involved gutters, street curbs, and sidewalks (Fig. 8). The longitudinal profile (A1-A2) revealed that the 10-m LiDAR DEM captured the overall northward inclination of this street section. However, this 10-m DEM presented the street surface as discrete steps. In contrast, the DEMs with higher resolutions were able to capture the subtle elevation variations, as confirmed by the RTK measurements. The transversal profiles (B1-B2, C1-C2, D1-D2) highlighted even smaller elevation variations. The 1-m LiDAR DEM generally concurred with the ground truth. The 1-m LiDAR DEM was able to indicate the shape of the street crown, but it could not capture the locations of street gutters. For example, there was a 1-m shift of the street gutter on the east side shifts in profile D1-D2. Such inaccurate delineation of street structures could lead to errors in the estimation of street width and associated hydrological responses. In both longitudinal and transversal profiles, the UAS DEMs appeared to perform better than coarse-resolution DEMs in describing the targeted features of urban microtopography.

In the second validation, the 10-m LiDAR DEM was unable to accurately depict the non-vegetated depression and the slope, as shown in Fig. 9. The 1-m LiDAR DEM also did not perform well in capturing the depth of the depression, especially on the profiles G1-G2 and H1-H2. In

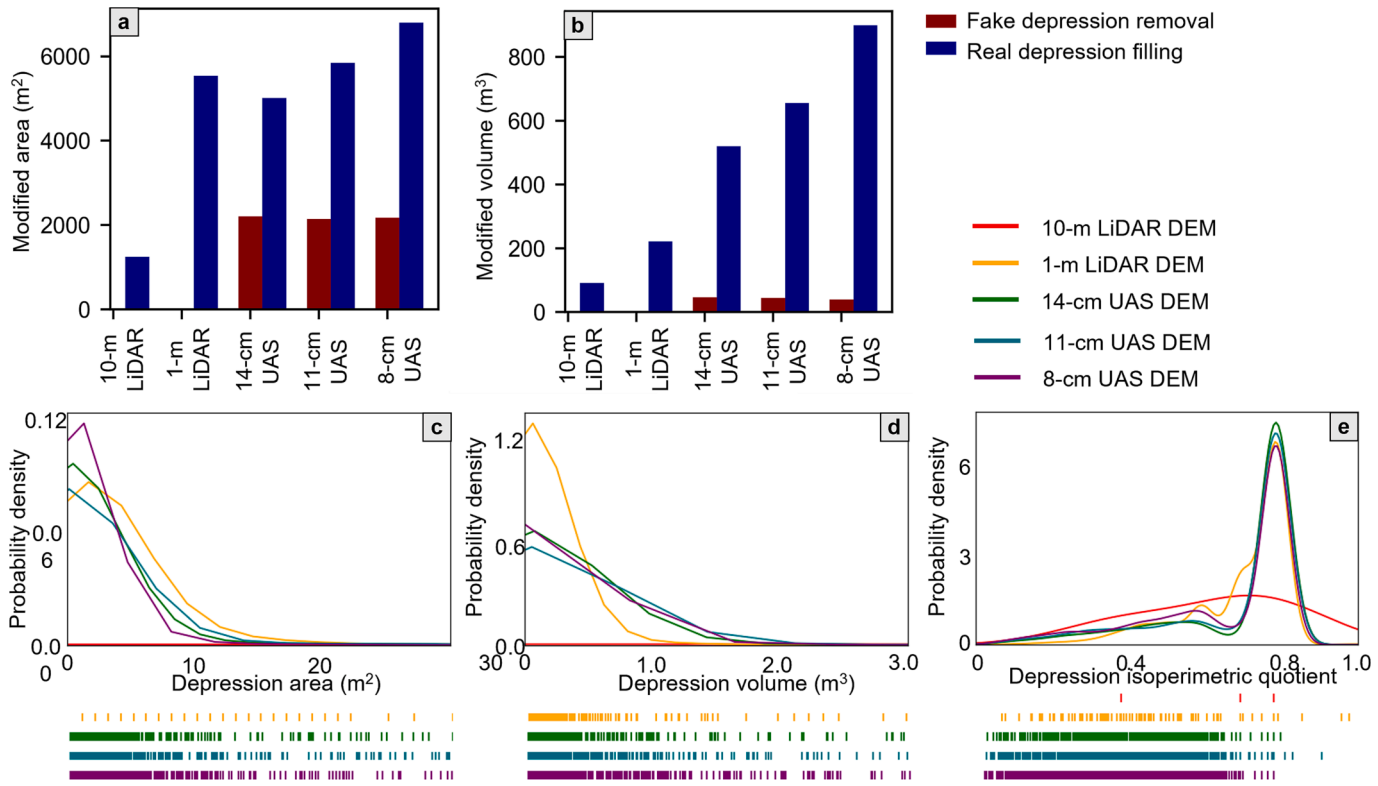

Fig. 5. The effects of the DEM sources on the depression characteristics: (a) modified area of DEMs; (b) modified volume of DEMs; (c) PDF of depression area; and (d) PDF of depression volume; (e) PDF of depression isoperimetric quotient.

Table 2
Depression and catchment area characteristics and network delineation.

			8-cm UAS DEM	11-cm UAS DEM	14-cm UAS DEM	1-m LiDAR DEM	10-m LiDAR DEM
Depression and catchment area characteristics	No. of depressions		4125	2457	1950	1385	3
	Largest depression area (m^2)		663.63	653.48	373.15	489	961.34
	Average depression area (m^2)		1.65	2.38	2.57	4	416.58
	No. of depressions		4123	2454	1948	1364	3
	Largest depression volume (m^3)		160.22	133	86.02	35.26	77.87
	Average depression volume (m^3)		0.22	0.27	0.27	0.16	30.44
	No. of catchments area		50	33	22	25	18
	Highest depression storage of catchment area (mm)		24.99	23.24	16.98	12.92	1.92
Network delineation	Total length (m)		8101.53	8002.74	7841.72	10080.39	10273.53
	Average length of link (m)		30.8	28.9	30.16	26.25	30.49
	1st order links	Average length of link (m)	31.44	28.51	28.76	25.98	33.53
		Total length (m)	4717.29	4560.9	4314.06	5638.28	6873.99
	2nd order links	Average length of link (m)	36.4	33.54	35.34	26.55	23.81
		Total length (m)	1383.47	1207.61	1272.25	1380.74	1095.18
	Maximum Shreve order	Order	55	54	58	53	38
		Average length of link (m)	7.33	8.35	11.48	14.44	6.93
		Total length (m)	7.33	8.35	11.48	14.44	6.93
	Primary flow direction	Orientation	N	N	N	N	N
		Total length (m)	2762.09	2756.35	2581.65	3568	4397.42
	Secondary flow direction	Orientation	NE	NE	NE	NE	NE
		Total length (m)	1366.37	1360.41	1366.93	1687.16	1767.92

comparison, the profiles of the 8.0-cm, 11.1-cm, and 13.6-cm DEMs mostly agreed with the ground truth. Only the profile adjacent to the curb (A1-A2) had lower reliability due to the obstructing images by the curb.

In the third validation, the 10-m LiDAR DEM did not capture the vegetated depression, as shown in Fig. 10. In comparison, the 1-m LiDAR DEM provided false topography over the longitudinal profile (A1-A2). The 1-m LiDAR DEM depicted an uneven surface, but the ground truth did not. The lowest position of the depression was flattened (the distance between 2 and 4 m of the A1-A2 profile). In addition, the profiles B1-B2 and C1-C2 showed that the depression was shallower than the ground truth and other UAS DEMs. While the UAS DEMs performed better than the coarse-resolution DEMs over the vegetated surface, the elevations from the DEMs were slightly higher than the ground truth. This may

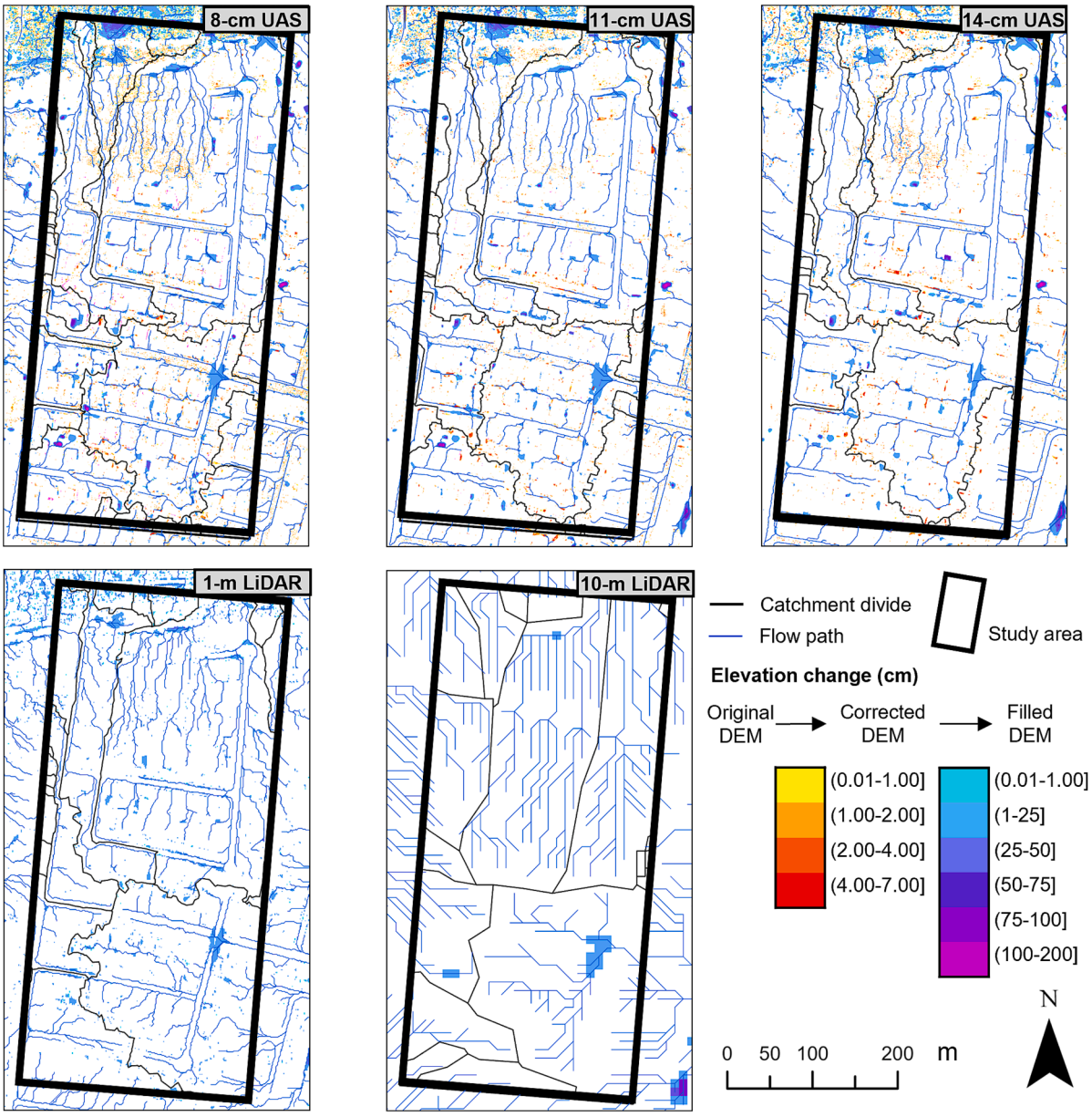

Fig. 6. The spatial pattern of the identified depressions in different DEMs. Blue lines are the results of flow accumulation, and different colors indicate elevation changes during correction and filling. (For interpretation of the references to color in this figure legend, the reader is referred to the web version of this article.)

have been due to the challenge of classifying dense vegetation near the surface from the ground.

Examples of several locations of standing water, identified through visual validation after a rainfall event, are shown in Fig. 11. The extent of the standing water reflected the shapes of the depressions, such as circular-shaped potholes on the streets or elongate-shaped depressions along the street gutters. As expected, all observed spots of standing water agreed with the depressions identified from the UAS DEMs. However, some small depressions filtered out during the DEM correction were confirmed to be true depressions in the field observation (e.g., the red-yellow areas in the results from 11-cm UAS DEM and 14-cm UAS DEM in Fig. 11). This indicates that removing fake depressions using RMSE could be improved by incorporating the spatial variations of the vertical accuracy.

3.4. Impacts of surface depression on runoff

Fig. 12 compares the runoff estimates from different DEMs across a range of design storms, highlighting the impact of depression storage on initial abstraction during runoff generation and routing. The 10-m LiDAR DEM has the lowest depression storage (with some catchments not having any storage), resulting in the highest direct runoff. More depressions are identified with a higher DEM resolution, leading to higher depression storage and, thus, reduced runoff. The effect of the DEM resolution on the runoff estimate is significant. For example, the runoff depth based on the 8-cm DEM was 41% lower than the 10-m LiDAR DEM estimation under a 2-year design storm. This effect, however, tends to be smaller with rare events. For example, the runoff estimation difference was only 13% under the 200-year design storm.

More importantly, runoff estimates based on UAS DEMs are within the range defined by standard I_a values (i.e., 5% and 20% of the maximum retention capacity S), while runoff estimates based on LiDAR DEMs are outside that range. This finding highlights the importance of carefully considering depressions in urban areas and their impact on runoff generation. More accurate runoff estimates can be obtained by choosing an appropriate initial abstraction value based on the specific

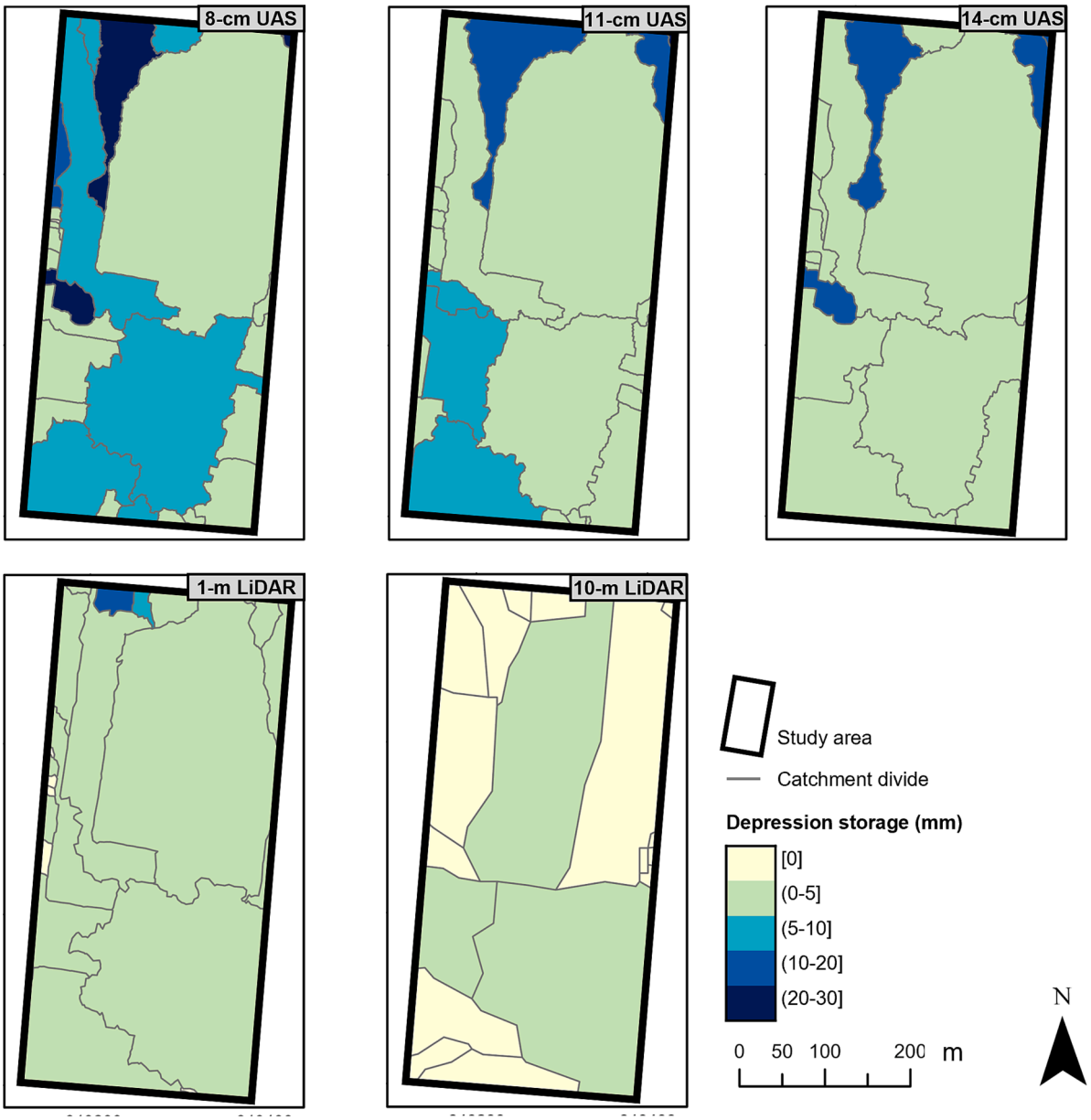

Fig. 7. Catchment depression storage.

characteristics of the study area and DEM resolution. The results indicate a critical role of surface depressions in urban hydrological models. Moreover, our findings highlight the importance of selecting a locally appropriate initial abstraction value that closely corresponds to the depression storage in the study area. This can lead to more accurate runoff estimates in urban catchments with a high density of depressions, especially for frequent events.

4. Discussion

4.1. Performance of existing DEMs

DEMs generated from manned aircraft, such as the 10-m LiDAR and 1-m LiDAR DEMs, offer more extensive coverage but are captured at high altitudes. This affects their ability to capture small urban topographical features. Our study indicates that the 10-m LiDAR DEM struggles to capture small depressions and depression storage capacity. Though it captures some large depressions, the estimates of their sizes and storage capacities are not reliable. Moreover, the 10-m LiDAR DEM cannot accurately describe street microtopography and produces unrealistic flow paths across the street, gutters, and sidewalks. This could significantly affect the DEM-based calculation of runoff flow paths, leading to misrepresenting runoff behaviors and introducing considerable uncertainty into hydrological modeling.

The 1-m LiDAR DEM performed considerably better than the 10-m LiDAR DEM. This DEM captured more depressions and better illustrated urban topographical features, such as the catchment divide along the street crown. However, the 1-m LiDAR DEM still cannot accurately reflect the actual size and depth of observed depressions shown in Fig. 11. The uncertainty of such depressions, especially on impervious surfaces, could be a significant cause of the miss-calibration of hydrological models (Zakizadeh et al., 2022).

4.2. Performance of UAS-generated DEMs

UAS DEMs have limited coverage. However, they are captured at low altitudes, allowing them to offer a more realistic description of urban watershed terrain than the manned aircraft DEMs. The UAS DEMs

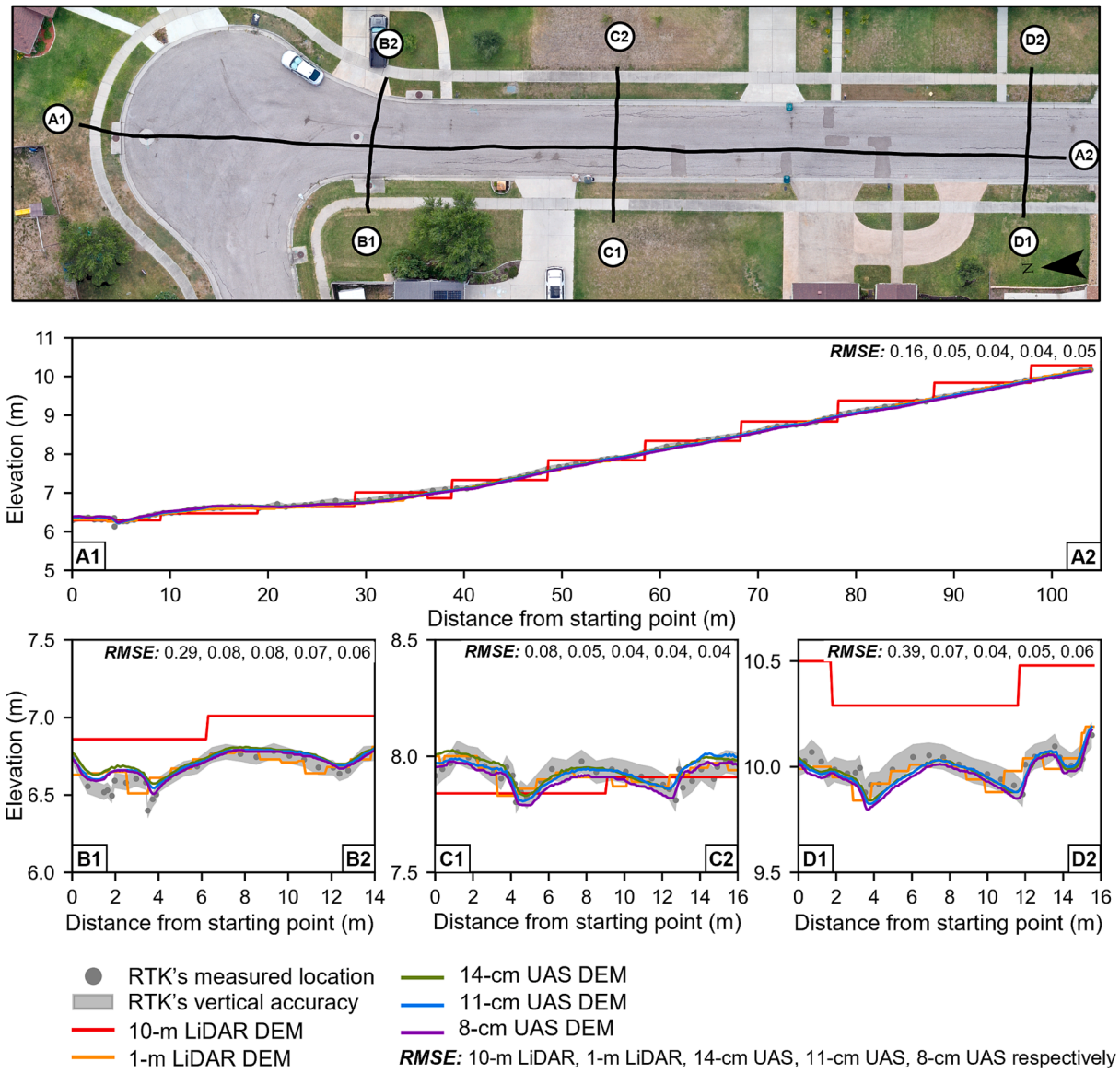

Fig. 8. Examples of street profiles. A1-A2 indicates the longitudinal section. B1-B2, C1-C2, and D1-D2 indicate the transversal sections. In each profile subplot, the values of RMSE are shown for all five DEMs.

detected more depressions than other DEMs. The detected depressions agreed well with the field measurements and observations (with a few exceptions explained in section 4.3). The fine-resolution DEMs also provided a higher estimate of the total volume of depression than the coarse-resolution DEMs.

More importantly, the UAS DEMs captured small topographical features, such as street crowns, street gutters, and sidewalks, which can significantly impact surface flow pathways and hydrological connectivity at the local scale. For example, the improved representation of street gutters in UAS-generated DEMs can help to simulate stormwater accurately flow along these features, ultimately leading to a more precise understanding of urban flooding patterns. Similarly, the ability of UAS DEMs to capture details like sidewalk elevations allows for better predictions of how stormwater runoff will interact with pedestrian infrastructure, providing valuable information for urban planners and stormwater management professionals.

The enhanced resolution of UAS DEMs also enables the identification of small-scale catchment divides, such as those found between buildings or on rooftops. This information is critical for simulating stormwater flow in densely built environments, where numerous structures can create complex and interconnected flow patterns. By accurately representing these catchment divides, researchers can better understand urban hydrological connectivity and develop targeted strategies for mitigating flood risks.

4.3. Limitations of UAS-generated DEMs

Despite the advantages of UAS-generated DEMs, caution is necessary for several reasons. First, the DEM-based drainage analysis cannot consider subsurface pathways (e.g., a stormwater sewer pipe) or overhead structures (e.g., a bridge). The filling procedure can create unrealistic flow pathways in such locations. The calculated runoff pathway is based on an adjusted terrain after the depressions are filled and may not align with the actual runoff pathways. Notably, in this study, the calculated total volumes of depressions (Fig. 5b) included all depressions regardless of whether they were hydraulically connected to the underground drainage system or not. The depressions hydraulically connected to the stormwater inlets do not retain the runoff unless the inlet is flooded. Fig. 13a illustrates two large depressions connected to the street inlets. These two depressions could be excluded from the

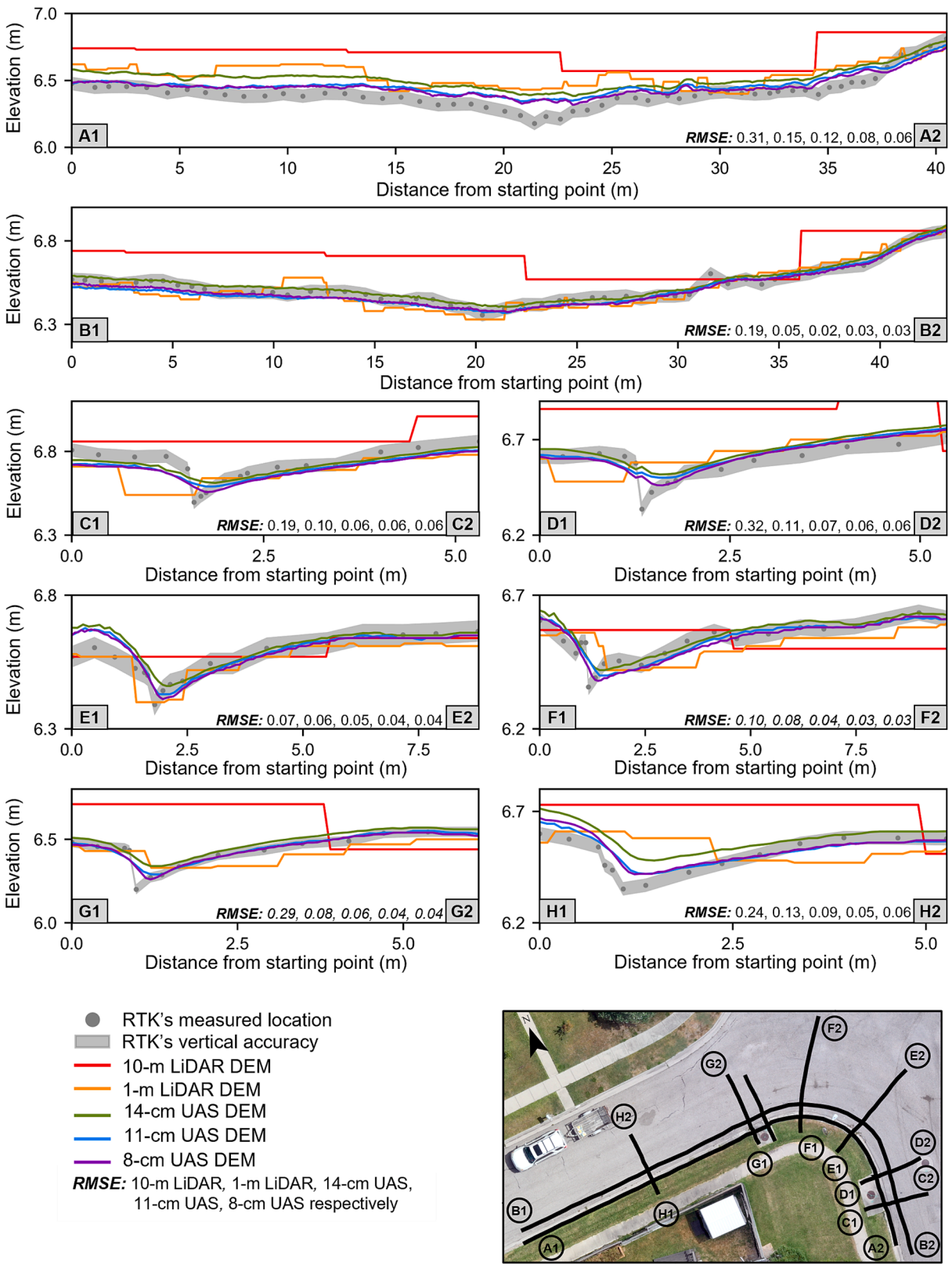

Fig. 9. Examples of the elevation profiles of non-vegetated depressions. In each profile subplot, the values of RMSE for this section are shown for all five DEMs.

depression storage calculation because they would not retain stormwater. Therefore, the total depression storage capacity could be classified based on the presence of the underground drainage system. Filling without considering the three-dimensional structure and underground drainage system can overestimate runoff at the local scale and the total depression storage capacity at the watershed scale. Integrating the dual-drainage concept, sewer, and overland flow (Maksimovic et al., 2009) could improve urban drainage models and enhance urban runoff assessments, benefiting further research in this area.

Second, trees may obstruct the visibility of UAS to capture street

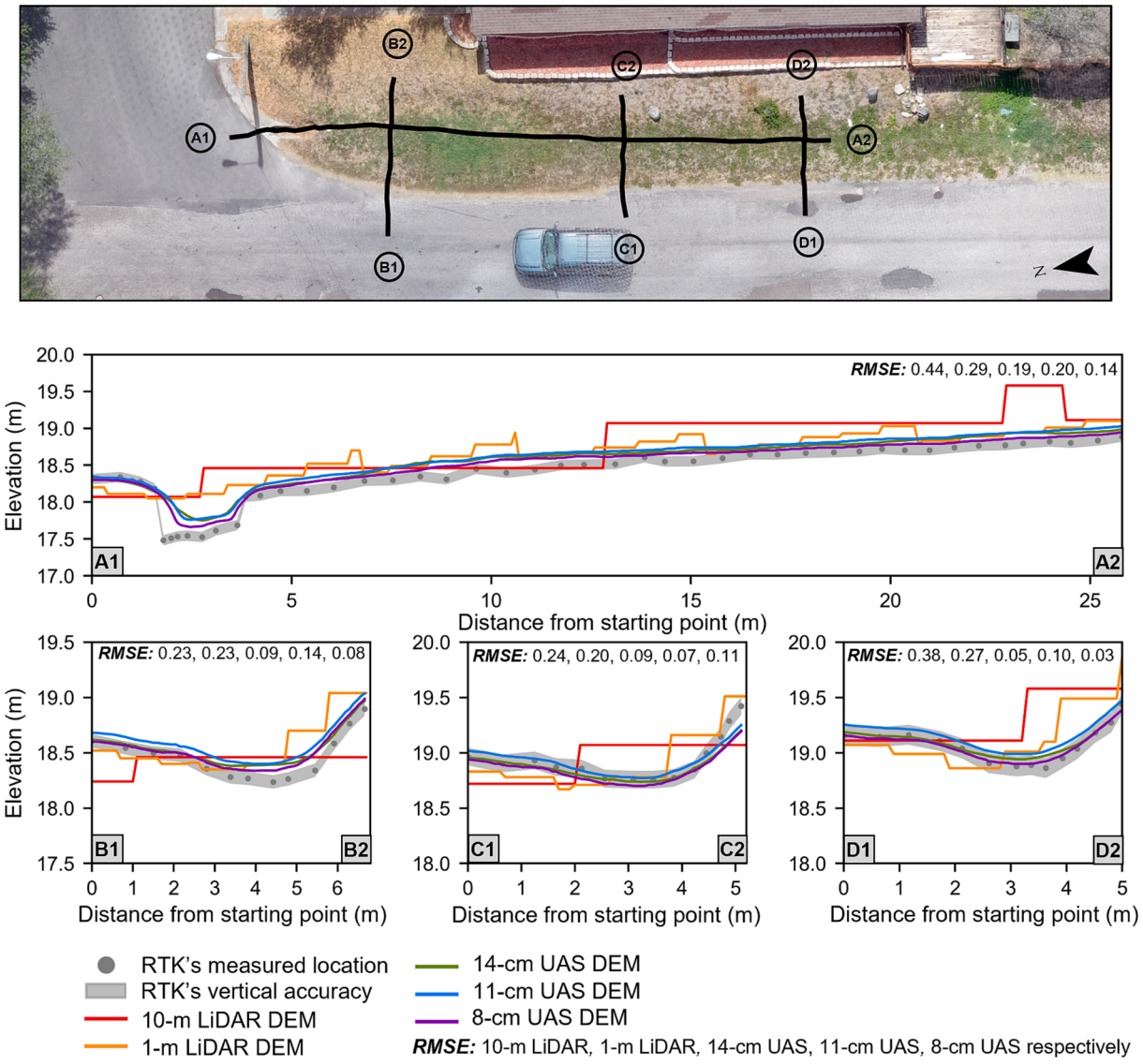

Fig. 10. Examples of the elevation profiles of vegetated depressions. In each profile subplot, the values of RMSE for this section are shown for all five DEMs.

gutters - the primary runoff pathway in an urban area, creating an unrealistic terrain. The areas under trees could create artifact depressions and incorrect flow routing. Moreover, other obstructive objects include cars and trash cans frequently seen on the streets over the street gutters. Even when some of these objects are eliminated during the construction of a DTM, the bare ground surface can still show the residues of some removed objects. Such residues are often hardly visible but could create artifact depressions and incorrect flow paths, as shown in Fig. 13b. The drainage analysis does not perform well in areas that are unclear of such obstructive objects. Therefore, UAS imaging missions should be designed to capture the study area comprehensively.

Third, the UAS did not perform well over open water. In particular, the inconsistent delineation of swimming pools with water led to uncertainties about their remaining volume for stormwater. For example, Fig. 13c shows considerable disagreement in the depth of depression from three different DEMs, leading to an incorrect calculation of the swimming pool's remaining storage capacity. The 8-cm UAS DEM gave a 1–2 m depression depth, but the 14-cm UAS DEM gave a smaller depth. The observation of three DEMs generated by UAS with different operational altitudes provided significant discrepancy in depression depth, i.e., 25–200 cm from 8-cm UAS DEM and 1–25 cm from 14-cm UAS DEM. This discrepancy affected the total depression volume in the study area, which is why the modified area required for filling is nearly equal, but the modified volume required for 8-cm UAS DEM is considerably higher than for 14-cm UAS DEM.

Fourth, DEM-derived depressions that are close to the canopy are more likely to be fake because the extent of the canopy usually obstructs the view of the UAS to detect the ground surface. For example, the highlighted areas (the blue areas) in Fig. 13d were identified as true depressions in the UAS DEMs, but were all found fake in the field validation. In contrast, LiDAR DEM did not create these fake depressions as significant as UAS-photogrammetry DEMs. However, efforts have been made to improve the accuracy of DEMs in densely vegetated areas, such as the proposed object-oriented classification ensemble algorithm for terrain correction (Meng et al., 2017) and the algorithm to assess flight mission settings for UAV-based photogrammetry using a custom-built simulator (Pessacg et al., 2022). These techniques could potentially be applied to urban runoff management to improve the accuracy of DEMs in areas with dense vegetation or other obstructive objects. Therefore, special attention should be given to densely vegetated areas when the UAS-photogrammetry DEMs for digital drainage analysis.

Lastly, the artifact removal method using RMSE could be improved. In this study, the elevation differences between DEM estimations and ground truth from 127 checkpoints were averaged into a single value of

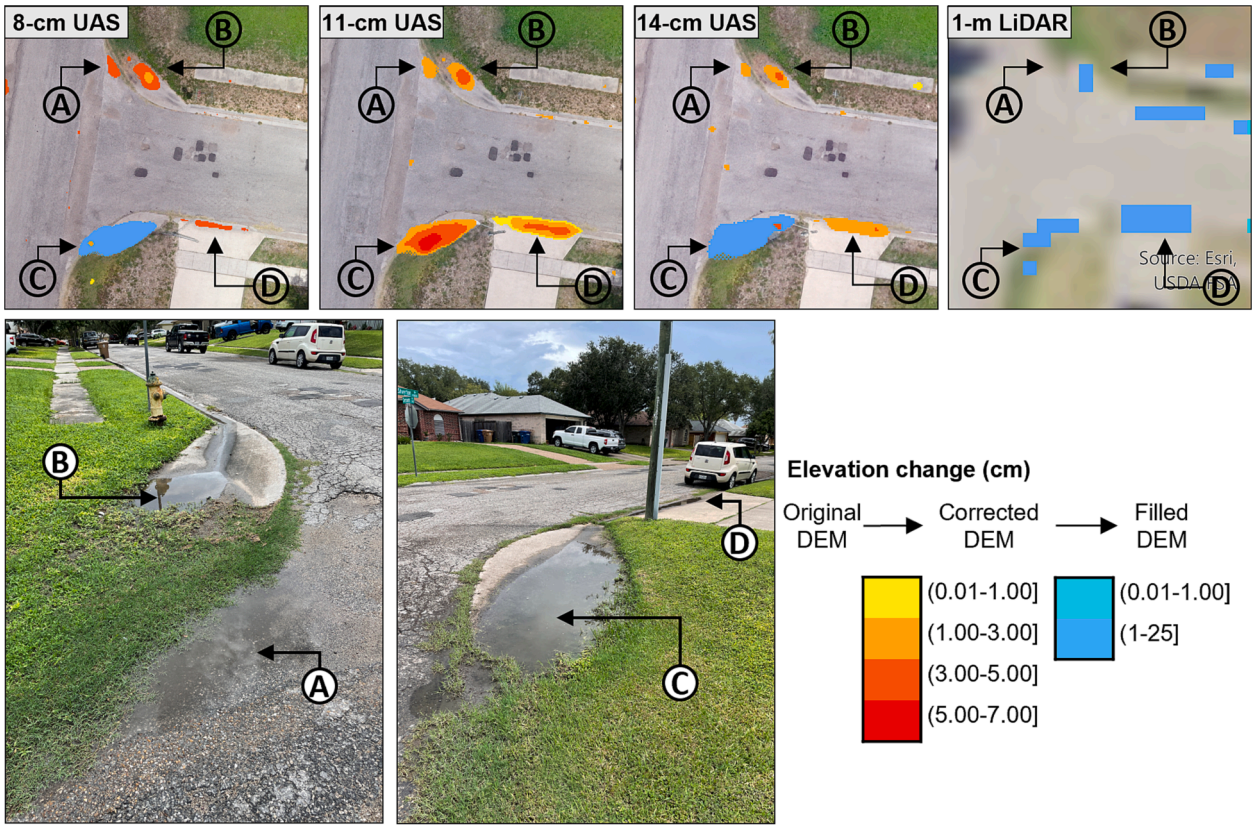

Fig. 11. Examples of the results from the visual inspections of DEM-derived depressions after a rainfall event.

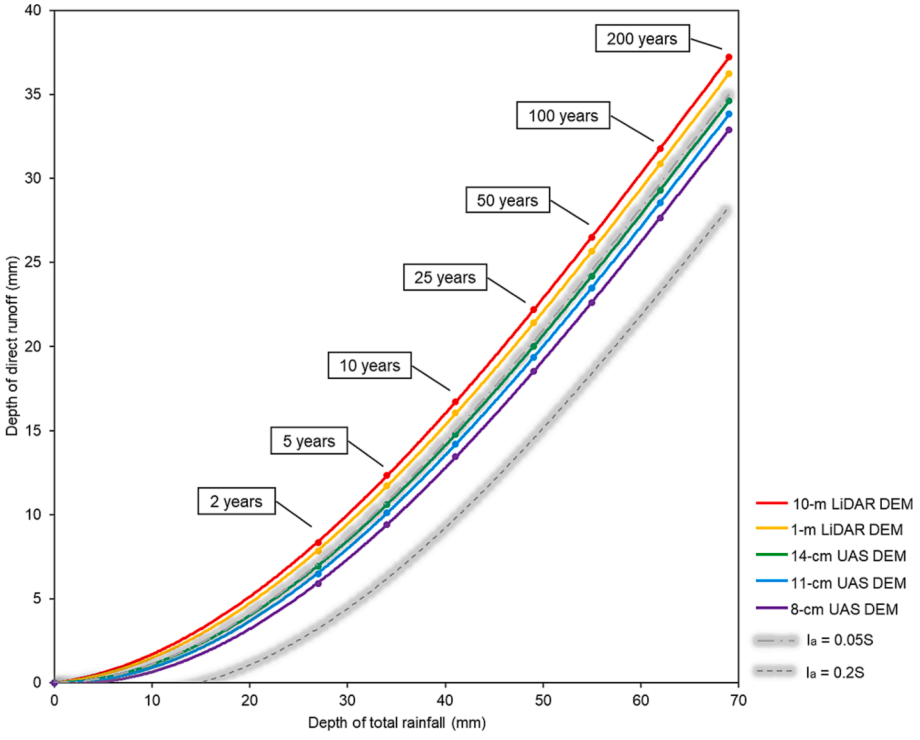

Fig. 12. Impacts of different DEM-derived estimates of depression storage on runoff across different design storms.

RMSE to represent the overall vertical accuracy of the entire study site. Some areas, e.g., pavements, may have relatively higher accuracy, so some corrected small depressions might be true features. These uncertainties in capturing depressions among UAS DEMs are from the performance of detecting features vertically. Although the results from 127 checkpoints reveal that three UAS-generated DEMs had similar

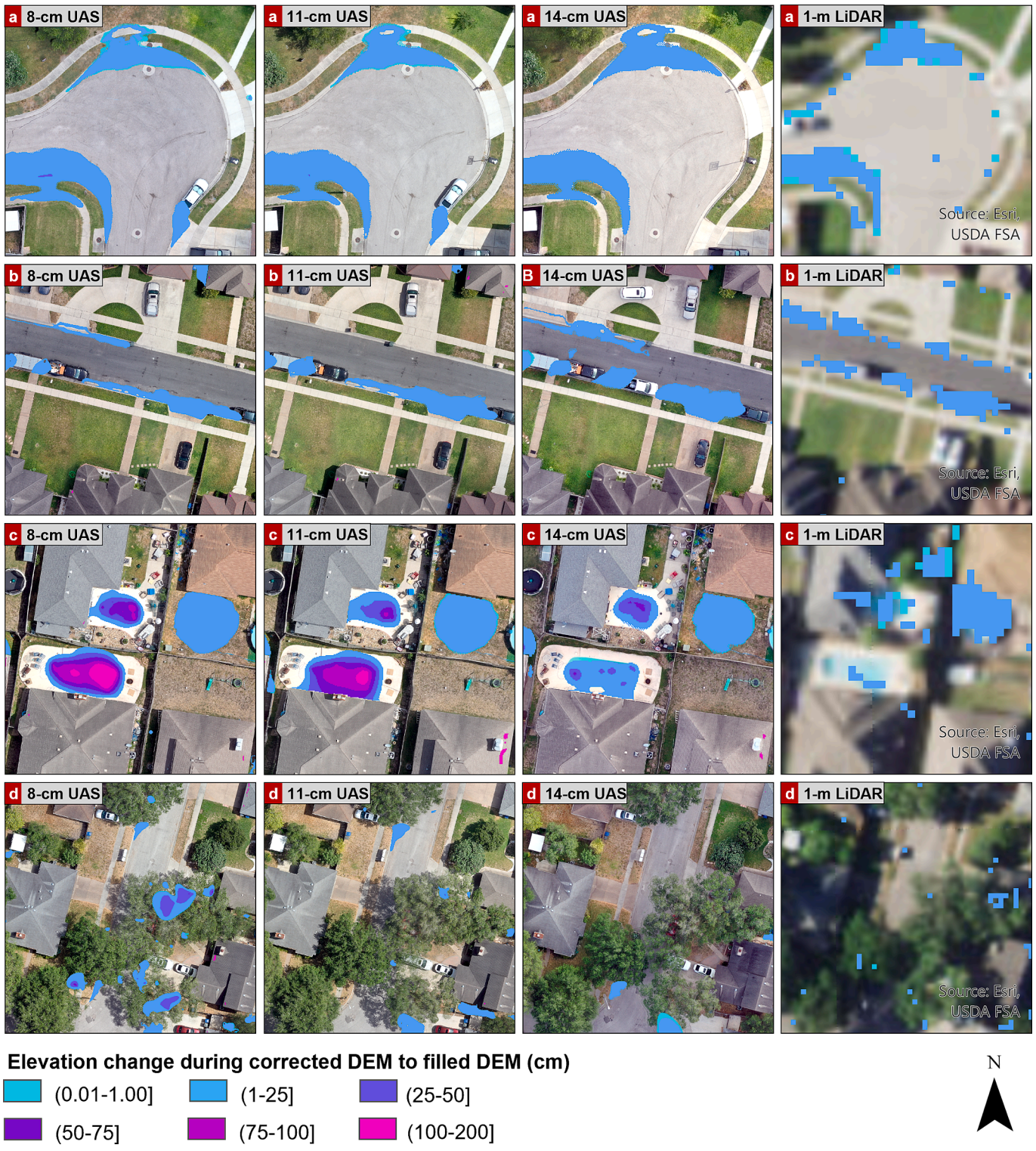

Fig. 13. Examples of urban areas that could have overestimated depression volumes: (a) hydraulically connected to an underground drainage system; (b) cars and trash cans; (c) swimming pool; and (d) vegetation.

RMSEs, the 127 checkpoints may not fully address the spatial variation of the vertical accuracy, particularly at a small scale. In addition, fake depression removal using the filling method only removes fake depression. However, it does not correct the geometry of the real depression presented on the DEMs to match the real-world topography.

4.4. Selecting appropriate DEMs for runoff estimation

Selecting the appropriate DEM for accurate runoff estimates is crucial and depends on various factors, including the study area's characteristics, resource availability, the required accuracy, and the targeted design storm. Especially when estimating runoff from frequent events (e.g., 2- and 5-year design storms), the amount of runoff generated is influenced by the topography and the capacity of depressions to

store rainfall. In these scenarios, runoff may not be generated if the rain does not exceed the depression storage capacity. Therefore, accurately accounting for depression storage is critical, as it helps determine the threshold at which runoff generation begins after depressions are filled. The UAS DEMs with centimeter resolutions are generally suitable for hydrological studies in urban areas with complex terrain and numerous small-scale features.

However, the UAS DEMs may not be suitable for large catchments due to their limited coverage or extreme events with long return periods. The time and resources required to collect extensive high-resolution data may become prohibitive. The finer details captured by UAS DEMs may not significantly impact the overall runoff estimates for larger catchments or more extreme events. As the spatial extent of the study area increases or the focus shifts towards less frequent, high-magnitude events, the advantages of UAS DEMs in capturing small-scale topographic features may become less critical to the overall accuracy of the hydrological modeling. In these scenarios, the hyperspatial resolution data provided by UAS DEMs may not justify the additional effort and cost required for data collection and processing.

Moreover, UAS DEMs may not always guarantee the accurate representation of real depressions, as they can still generate fake depressions. While eliminating fake depressions in small study areas may be feasible, this becomes more challenging when applying UAS DEMs to large-scale areas. In these scenarios, it is not guaranteed that all depressions will be real, and the additional effort to identify and remove fake depressions may not be practical or efficient.

Considering these limitations, researchers may opt for more effective DEMs, such as those generated by manned aircraft, which offer higher coverage and require fewer data collection and processing resources. These DEMs, such as 1-m LiDAR DEMs (for this study), strike a balance between resolution and coverage, making them suitable for a broader range of applications, including long recurrence period events where percentage estimates may not significantly differ between UAS and airborne DEMs. The choice of DEM should ultimately align with the specific objectives and requirements of the study. By recognizing the limitations and advantages of each DEM type, researchers can make informed decisions and enhance the accuracy of their runoff estimates, mainly when accounting for depression storage and its influence on runoff generation.

5. Conclusions

In this study, UAS-photogrammetry DEMs captured depressions more effectively than the existing DEMs acquired by manned aircrafts. The UAS DEMs led to higher estimates in both the number of depressions and their storage capacity compared to results from the existing DEMs. UAS DEMs were able to distinguish urban microtopographic features and described small depressions with good agreement with field validations, but the results still included fake depressions, particularly in areas affected by vegetation, 3D structures, and temporary objects on the streets. Additionally, the DEM resolution affected the derived hydrological attributes, including the flow direction, flow accumulation, and catchment boundaries. Our results suggest that existing DEMs are not the appropriate input for estimating urban runoff from frequent events with low rainfall amounts, as they tend to exclude small depressions storage.

UAS has been widely applied worldwide in various urban stormwater management studies. It is essential to acknowledge that the high resolution of UAS photogrammetry data does not guarantee an accurate description of the complex terrain and landscape of an urban watershed and the derived hydrological attributes. Urban stormwater management studies should consider the reliability of DEM-derived depressions before further analysis. Future research should improve high-resolution depression classification methods, emphasizing filtering fake depressions in high-resolution DEM data. This includes an improved understanding of the interconnectedness between DEM resolution, hydrological characteristics, and the fractal nature of surface topography. Such advances will contribute significantly to improving the precision of urban hydrological modeling and further expanding the utility of UAS in urban hydrology and water management.

CRediT authorship contribution statement

Lapone Techapinyawat: Conceptualization, Methodology, Data curation, Formal analysis, Writing – original draft, Writing – review & editing. **Ian Goulden-Brady:** Methodology, Data curation. **Hannah Garcia:** Methodology, Data curation. **Hua Zhang:** Conceptualization, Funding acquisition, Methodology, Writing – review & editing.

Declaration of Competing Interest

The authors declare that they have no known competing financial interests or personal relationships that could have appeared to influence the work reported in this paper.

Data availability

Data will be made available on request.

Acknowledgments

This work was supported by the National Science Foundation (NSF) under grant 2050986 to Texas A&M University-Corpus Christi. Any opinions, findings, conclusions, or recommendations expressed in this material are those of the authors and do not necessarily reflect the view of NSF. We thank Icograms (icograms.com) for providing services and materials in the development of Fig. 1.

References

Abd Elbasit, M.A.M., Abu-Zreig, M.M., Ojha, C.S.P., Yasuda, H., Gang, L., 2020. Estimation of surface depression storage capacity from random roughness and slope. Water SA 46 (3), 404–409. https://doi.org/10.17159/wsa/2020.v46.i3.8650.

Abdelkarim, A., Gaber, A.F.D., Youssef, A.M., Pradhan, B., 2019. Flood Hazard Assessment of the Urban Area of Tabuk City, Kingdom of Saudi Arabia by Integrating Spatial-Based Hydrologic and Hydrodynamic Modeling. Sensors-Basel 19 (5). https://doi.org/10.3390/s19051024.

Abedini, M.J., Dickinson, W.T., Rudra, R.P., 2006. On depressional storages: The effect of DEM spatial resolution. J. Hydrol. 318 (1), 138–150. https://doi.org/10.1016/j.jhydrol.2005.06.010.

Acharya, B.S., Bhandari, M., Bandini, F., Pizarro, A., Perks, M., Joshi, D.R., Wang, S., Dogwiler, T., Ray, R.L., Kharel, G., Sharma, S., 2021. Unmanned Aerial Vehicles in Hydrology and Water Management: Applications, Challenges, and Perspectives. Water Resour. Res. 57 (11) https://doi.org/10.1029/2021WR029925.

Aguera-Vega, F., Aguera-Puntas, M., Martinez-Carricondo, P., Mancini, F., Carvajal, F., 2020. Effects of point cloud density, interpolation method and grid size on derived Digital Terrain Model accuracy at micro topography level. Int. J. Remote Sens. 41 (21), 8281–8299. https://doi.org/10.1080/01431161.2020.1771788.

Becker, C., Rosinskaya, E., Hani, N., d'Angelo, E., Strecha, C., 2018. Classification of Aerial Photogrammetric 3D Point Clouds. Photogramm Eng Rem S 84 (5), 287–295. https://doi.org/10.14358/PERS.84.5.287.

Callaghan, K.L., Wickert, A.D., 2019. Computing water flow through complex landscapes - Part 1: Incorporating depressions in flow routing using FlowFill. Earth Surf Dynam 7 (3), 737–753. https://doi.org/10.5194/esurf-7-737-2019.

City of Corpus Christi GIS Services, 2018. City of Corpus Christi Land Use. City of Corpus Christi.

Cordonnier, G., Bovy, B., Braun, J., 2019. A versatile, linear complexity algorithm for flow routing in topographies with depressions. Earth Surf Dynam 7 (2), 549–562. https://doi.org/10.5194/esurf-7-549-2019.

Cuartero, A., Felicisimo, A.M., Ariza, F.J., 2005. Accuracy, reliability, and depuration of SPOT HRV and Terra ASTER digital elevation models. IEEE Trans. Geosci. Remote Sens. 43 (2), 404–407. https://doi.org/10.1109/TGRS.2004.841356.

Darboux, F., Davy, P., Gascuel-Odoux, C., 2002. Effect of depression storage capacity on overland-flow generation for rough horizontal surfaces: Water transfer distance and scaling. Earth Surf. Proc. Land. 27 (2), 177–191. https://doi.org/10.1002/esp.312.

Dell, T., Razzaghmanesh, M., Sharvelle, S., Arabi, M., 2021. Development and Application of a SWMM-Based Simulation Model for Municipal Scale Hydrologic Assessments. Water-Sui 13 (12). https://doi.org/10.3390/w13121644.

Deng, J., Yin, H., Kong, F., Chen, J., Dronova, I., Pu, Y., 2020. Determination of runoff response to variation in overland flow area by flow routes using UAV imagery. J. Environ. Manage. 265, 109868.

Escobar Villanueva, J.R., Iglesias Martínez, L., Pérez Montiel, J.I., 2019. DEM Generation from Fixed-Wing UAV Imaging and LiDAR-Derived Ground Control Points for Flood Estimations. Sensors 19 (14), 3205. https://doi.org/10.3390/s19143205.

Gao, J.A.Y., 1997. Resolution and accuracy of terrain representation by grid DEMs at a micro-scale. Int. J. Geogr. Inf. Sci. 11 (2), 199–212. https://doi.org/10.1080/136588197242464.

Habtezion, N., Nasab, M.T., Chu, X.F., 2016. How does DEM resolution affect microtopographic characteristics, hydrologic connectivity, and modelling of hydrologic processes? Hydrol. Process. 30 (25), 4870–4892. https://doi.org/10.1002/hyp.10967.

Hu, L., Bao, W., Shi, P., Wang, J., Lu, M., 2020. Simulation of overland flow considering the influence of topographic depressions. Sci. Rep. 10 (1), 6128. https://doi.org/10.1038/s41598-020-63001-y.

Jenson, S.K., Domingue, J.O., 1988. Extracting Topographic Structure from Digital Elevation Data for Geographic Information-System Analysis. Photogramm Eng Rem S 54 (11), 1593–1600.

Jiménez-Jiménez, S.I., Ojeda-Bustamante, W., Marcial-Pablo, M.d.J., Enciso, J., 2021. Digital Terrain Models Generated with Low-Cost UAV Photogrammetry: Methodology and Accuracy. ISPRS Int. J. Geo Inf. 10 (5), 285. https://doi.org/10.3390/ijgi10050285.

Krajewski, A., Sikorska-Senoner, A.E., Hejduk, A., Hejduk, L., 2020. Variability of the Initial Abstraction Ratio in an Urban and an Agroforested Catchment. Water-Sui 12 (2). https://doi.org/10.3390/w12020415.

Leitao, J.P., Boonya-Aroonnet, S., Prodanovic, D., Maksimovic, C., 2009. The influence of digital elevation model resolution on overland flow networks for modelling urban pluvial flooding. Water Sci. Technol. 60 (12), 3137–3149. https://doi.org/10.2166/wst.2009.754.

Leitao, J.P., de Vitry, M.M., Scheidegger, A., Rieckermann, J., 2016. Assessing the quality of digital elevation models obtained from mini unmanned aerial vehicles for overland flow modelling in urban areas. Hydrol Earth Syst Sc 20 (4), 1637–1653. https://doi.org/10.5194/hess-20-1637-2016.

Lindsay, J.B., Creed, I.F., 2005. Removal of artifact depressions from digital elevation models: towards a minimum impact approach. Hydrol. Process. 19 (16), 3113–3126. https://doi.org/10.1002/hyp.5835.

Lindsay, J.B., Creed, I.F., 2006. Distinguishing actual and artefact depressions in digital elevation data. Comput. Geosci. 32 (8), 1192–1204. https://doi.org/10.1016/j.cageo.2005.11.002.

Maksimović, Č., Prodanović, D., Boonya-Aroonnet, S., Leitão, J.P., Djordjević, S., Allitt, R., 2009. Overland flow and pathway analysis for modelling of urban pluvial flooding. J. Hydraul. Res. 47 (4), 512–523.

McDonald, W., 2019. Drones in urban stormwater management: a review and future perspectives. Urban Water J. 16 (7), 505–518. https://doi.org/10.1080/1573062X.2019.1687745.

Meng, X., Shang, N., Zhang, X., Li, C., Zhao, K., Qiu, X., Weeks, E., 2017. Photogrammetric UAV Mapping of Terrain under Dense Coastal Vegetation: An Object-Oriented Classification Ensemble Algorithm for Classification and Terrain Correction. Remote Sens-Basel 9 (11), 1187.

Moore, I.D., Grayson, R.B., Ladson, A.R., 1991. Digital Terrain Modeling - a Review of Hydrological, Geomorphological, and Biological Applications. Hydrol. Process. 5 (1), 3–30. https://doi.org/10.1002/hyp.3360050103.

Nex, F., Armenakis, C., Cramer, M., Cucci, D.A., Gerke, M., Honkavaara, E., Kukko, A., Persello, C., Skaloud, J., 2022. UAV in the advent of the twenties: Where we stand and what is next. ISPRS J. Photogramm. Remote Sens. 184, 215–242.

Padro, J.C., Munoz, F.J., Planas, J., Pons, X., 2019. Comparison of four UAV georeferencing methods for environmental monitoring purposes focusing on the combined use with airborne and satellite remote sensing platforms. Int J Appl Earth Obs 75, 130–140. https://doi.org/10.1016/j.jag.2018.10.018.

Paton, E., Haacke, N., 2021. Merging patterns and processes of diffuse pollution in urban watersheds: A connectivity assessment. WIREs Water 8 (4), e1525.

Pessacg, F., Gómez-Fernández, F., Nitsche, M., Chamo, N., Torrella, S., Ginzburg, R., De Cristóforis, P., 2022. Simplifying UAV-Based Photogrammetry in Forestry: How to Generate Accurate Digital Terrain Model and Assess Flight Mission Settings. Forests 13 (2), 173.

Schumann, G.-J.-P., Muhlhausen, J., Andreadis, K.M., 2019. Rapid Mapping of Small-Scale River-Floodplain Environments Using UAV SfM Supports Classical Theory. Remote Sens. (Basel) 11 (8), 982. https://doi.org/10.3390/rs11080982.

Singh, C., Mishra, V., Harshit, H., Jain, K., Mokros, M., 2022. Application of Uav Swarm Semi-Autonomous System for the Linear Photogrammetric Survey. Int Arch Photogramm 43–B1, 407–413. https://doi.org/10.5194/isprs-archives-XLIII-B1-2022-407-2022.

Tonkin, T.N., Midgley, N.G., 2016. Ground-Control Networks for Image Based Surface Reconstruction: An Investigation of Optimum Survey Designs Using UAV Derived Imagery and Structure-from-Motion Photogrammetry. Remote Sens-Basel 8 (9). https://doi.org/10.3390/rs8090786.

Trepekli, K., Balstrøm, T., Friborg, T., Fog, B., Allotey, A.N., Kofie, R.Y., Møller-Jensen, L., 2022. UAV-borne, LiDAR-based elevation modelling: a method for improving local-scale urban flood risk assessment. Nat. Hazards 113 (1), 423–451.

USDA-SCS, 1986. Urban hydrology for small watersheds. Engineering Division, Soil Conservation Service, U.S. Dept. of Agriculture, [Washington, D.C.], 1 v. (various pagings) pp.

Velez-Nicolas, M., Garcia-Lopez, S., Barbero, L., Ruiz-Ortiz, V., Sanchez-Bellon, A., 2021. Applications of Unmanned Aerial Systems (UASs) in Hydrology: A Review. Remote Sens-Basel 13 (7). https://doi.org/10.3390/rs13071359.

Wang, N., Chu, X.F., 2020. A New Algorithm for Delineation of Surface Depressions and Channels. Water-Sui 12 (1). https://doi.org/10.3390/w12010007.

Wang, N., Chu, X., Zhang, X., 2021. Functionalities of surface depressions in runoff routing and hydrologic connectivity modeling. J. Hydrol. 593, 125870.

Wang, C., Gomez-Velez, J.D., Wilson, J.L., 2018. The Importance of Capturing Topographic Features for Modeling Groundwater Flow and Transport in Mountainous Watersheds. Water Resour. Res. 54 (12), 10313–10338. https://doi.org/10.1029/2018WR023863.

Wang, L., Liu, H., 2006. An efficient method for identifying and filling surface depressions in digital elevation models for hydrologic analysis and modelling. Int. J. Geogr. Inf. Sci. 20 (2), 193–213. https://doi.org/10.1080/13658810500433453.

Wu, Q., Lane, C.R., Wang, L., Vanderhoof, M.K., Christensen, J.R., Liu, H., 2019. Efficient Delineation of Nested Depression Hierarchy in Digital Elevation Models for Hydrological Analysis Using Level-Set Methods. J. Am. Water Resour. Assoc. 55 (2), 354–368.

Zakizadeh, F., Nia, A.M., Salajegheh, A., Sanudo-Fontaneda, L.A., Alamdari, N., 2022. Efficient Urban Runoff Quantity and Quality Modelling Using SWMM Model and Field Data in an Urban Watershed of Tehran Metropolis. Sustainability-Basel 14 (3). https://doi.org/10.3390/su14031086.

Zandbergen, P.A., 2010. Accuracy Considerations in the Analysis of Depressions in Medium-Resolution Lidar DEMs. Gisci Remote Sens. 47 (2), 187–207. https://doi.org/10.2747/1548-1603.47.2.187.

Zhang, S.H., Pan, B.Z., 2014. An urban storm-inundation simulation method based on GIS. J. Hydrol. 517, 260–268. https://doi.org/10.1016/j.jhydrol.2014.05.044.

Zhao, G., Mark, O., Balstrøm, T., Jensen, M.B., 2022. A Sink Screening Approach for 1D Surface Network Simplification in Urban Flood Modelling. Water-Sui 14 (6), 963. https://doi.org/10.3390/w14060963.